BSc thesis:
Regions of fresh water influence

The influence of depth on a ROFI

Silke Tas

Delft University of Technology

TU Delft Delft University of Technology

Challenge the future

Cover photo:

River plume at the outflow of the Fraser River in British Columbia, Canada.

NASA Earth Observatory image created by Robert Simmon and Jesse Allen,
using Landsat data provided by the United States Geological Survey.
http://earthobservatory.nasa.gov/IOTD/view.php?id=77368&src=eorss-iotd

REGIONS OF FRESH WATER INFLUENCE

THE INFLUENCE OF DEPTH ON A ROFI

BACHELOR THESIS

Silke Tas
4169905

July 2014

Supervision

Prof. dr. J.D. Pietrzak
Dr. ir. G.J. de Boer
Ir. S. Rijnsburger

Faculty of Civil Engineering – Delft University of Technology

ABSTRACT

The topic of this paper is the study of the tidal velocity profiles within a region of fresh water influence (referred to as ROFI in this paper). These regions of fresh water influence occur where rivers discharge fresh water into salty seas.

The main research question is how depth influences the behaviour of the tidal velocity profile in a region of fresh water influence.

The approach for this investigation is to apply a model to two different ROFI systems, and compare the results. The first system considered is the Rhine ROFI, for which numerous field data have been collected (Simpson, et al. 1993) and a numerical model has been created (de Boer, Pietrzak and Winterwerp 2006). The second system is the Fraser ROFI in Canada, having similar tidal characteristics as the Rhine ROFI (Foreman, et al. 1995), but a much larger depth. The model used for this comparison is an analytic model, based on Prandle (Prandle 1982a).

In order to do so, it was first necessary to understand the complex behaviour of the tidal velocity profile of the Rhine ROFI. The big difference between the behaviour for neap and spring tide can be explained by decomposing the tidal velocity vector into two counter rotating phasors. Also, two parameters turned out to be important: the depth-averaged velocity and the eddy viscosity.

As second goal, and main objective of this paper, was to study the impact of the depth on the behaviour of the tidal velocity profile in the region of fresh water influence. This was done by comparing the shallow Rhine ROFI with the much deeper Fraser ROFI. It turned out that finding realistic values for the eddy viscosity coefficient was the biggest challenge.

The ability of predicting vertical current profiles may serve many applications, such as offshore construction or oil leaks. Being able to apply this model to other ROFI's around the world with different depths, is therefore a very useful aim.

TABLE OF CONTENTS

1. INTRODUCTION

Every day, more and more companies launch projects offshore. With these projects comes the need for more detailed knowledge of the vertical structure of currents. For example, the construction of the new wind farm “Luchterduinen” off the Dutch coast: what will be the forces exerted by the current? When will be the optimal time to install the wind turbines? Another example is the disaster with the Deepwater Horizon offshore oil drilling rig. How will the oil spill evolve? Where will it flow to, how fast will it mix? These are situations where the general logarithmic profile no longer meets the requirements, and a thorough understanding of the vertical structure of currents is required.

All over the world rivers discharge into oceans and seas. Because of Earth’s rotation, the outflow turns to the right on the Northern hemisphere and follows the coast. The fresh water forms a river plume, which is also called a region of fresh water influence, or ROFI (Simpson, et al. 1993). Fresh water flowing on top of sea water causes vertical and horizontal density differences, which influence the current patterns. Contrary to the general idea of tidal currents, where the whole water mass moves in an alongshore direction, water particles at the surface may behave differently from water particles at 2/3 of the water depth. Water particles along the same vertical but at different depths, may have different velocity magnitudes and directions, and the vertical profile can differ completely from the often used logarithmic velocity profile.

The Rhine and Meuse river system discharges fresh river water into the North Sea, creating the Rhine region of fresh water influence (ROFI) in front of the Dutch coast. The Rhine is one of Europe’s major rivers, with an average discharge of 2500 m^3/s. In the North Sea, a semi-diurnal tide dominates, so a tidal cycle is about 12 hours long. Next to this semi-diurnal tide, there is also a semi-monthly spring/neap variation (de Boer, Pietrzak and Winterwerp 2006).

In September and October 1990, data were collected in the Rhine ROFI by Simpson et al. (Simpson, et al. 1993). These data proved the existence of the semi-diurnal tidal cycle with semi-monthly variation, with two times a day high and low tide and twice a month spring and neap tide. These data also showed other important characteristics of the vertical structure. During spring tide, the vertical water column is very well mixed except near the mouth of the Rhine. But during neap tide, the water column is stratified.

These different vertical structures have a big influence on the tidal current: during well-mixed conditions, the tidal currents are rectilinear, parallel to the coast; during stratified conditions, the tidal currents contain significant cross-shore components. In the latter case, the tidal motion becomes elliptic, and the ellipses at the surface rotate in the opposite direction of the ellipses at the bottom. The elliptic motion is a consequence of the fact that the tidal motion is composed of two counter rotating phasors. If the clockwise rotating phasor is dominating the other, this will result in an elliptic motion, rotating clockwise. If both phasors have (almost) the same amplitude, the resulting motion is rectilinear. The difference in elliptic behaviour for neap and spring tide is caused by stratification. Stratification shuts down the turbulence and therefore also changes the influence of boundary layers.

The objective of this Bachelor thesis is to explore the influence of depth on the region of fresh water influence. The model used for this investigation is an analytic Matlab model, written by de Boer and based on the analytic solution derived by Prandle (Prandle 1982a). The first goal is to obtain a thorough understanding of the complex behaviour in the Rhine ROFI. Only when fully understanding what happens at the Rhine ROFI, the influence of depth on a ROFI can be investigated, which is the second objective and main research goal. To study the impact of depth on the behaviour within a ROFI, two cases will be compared. The Rhine ROFI, as an example of a shallow situation, will be compared to the Fraser ROFI. The Fraser is a river in British Columbia, Canada, where it flows into the very deep Strait of Georgia. Comparing both cases will give insight in how depth can influence the vertical velocity structure in magnitude, direction and timing.

The report has been structured by explaining the necessary theory in chapter 2. Here the system of equations describing a ROFI is derived, together with the derivation of the analytic solution following Prandle´s work (Prandle 1982a). In chapter 3, the used model, an analytic Matlab model written by de Boer, based on Prandle´s solution, is described. The results obtained by using this model and the comparison between the Rhine ROFI and the Fraser ROFI are discussed in chapter 4. Conclusions and recommendations are given in chapter 5.

2. THEORY

2.1 SYSTEM OF EQUATIONS

The Rhine region of fresh water influence can be described using a system of six equations. First, the selection of a coordinate system. In this approach is opted for a Cartesian system (x, y, z), with the x-axis pointing towards the east, the y-axis pointing towards the north and the vertical z-axis pointing up, going from $-h(x, y, t)$ at the bottom to $\zeta(x, y, t)$ at the surface, where h is the average surface level and ζ is the surface elevation. There are six unknowns: the velocities in respectively the x, y and z direction, u, v and w, p the pressure and T and S, the temperature and salinity respectively. To solve for these six unknowns, six equations are needed. The continuity equation, three momentum equations (one in each direction of the Cartesian coordinate system) and two transport equations (one for heat and one for salinity) can be used. For the derivation of the following six equations, read appendix A: Derivation of the system of equations. Equation 1.1 represents the continuity equation, equation 1.2 to 1.4 the equations of motion and equations 1.5 and 1.6 represent the transport equations for salinity and temperature.

$$\begin{cases} equation\ 1: & \frac{\partial u}{\partial x} + \frac{\partial v}{\partial y} + \frac{\partial w}{\partial z} = 0,\ or \qquad \nabla \boldsymbol{V} = 0 \\ equation\ 2: & \frac{\partial u}{\partial t} + \frac{\partial u^2}{\partial x} + \frac{\partial uv}{\partial y} + \frac{\partial uw}{\partial z} - fv + \frac{1}{\rho_0}\frac{\partial p}{\partial x} - F_x - \frac{\partial}{\partial z}\left(E\frac{\partial u}{\partial z}\right) = 0 \\ equation\ 3: & \frac{\partial v}{\partial t} + \frac{\partial vu}{\partial x} + \frac{\partial v^2}{\partial y} + \frac{\partial vw}{\partial z} + fu + \frac{1}{\rho_0}\frac{\partial p}{\partial y} - F_y - \frac{\partial}{\partial z}\left(E\frac{\partial v}{\partial z}\right) = 0 \\ equation\ 4: & \frac{\partial p}{\partial z} = -\rho g \\ equation\ 5: & \frac{\partial S}{\partial t} + \frac{\partial uS}{\partial x} + \frac{\partial vS}{\partial y} + \frac{\partial wS}{\partial z} - F_S - \frac{\partial}{\partial z}\left(D_t\frac{\partial S}{\partial z}\right) = S_{SS} \\ equation\ 6: & \frac{\partial T}{\partial t} + \frac{\partial uT}{\partial x} + \frac{\partial vT}{\partial y} + \frac{\partial wT}{\partial z} - F_T - \frac{\partial}{\partial z}\left(D_t\frac{\partial T}{\partial z}\right) = \frac{1}{\rho}Q_H + S_{SS} \end{cases} \quad [1]$$

2.2 Analytic solution by Prandle

The next step is to derive an analytic solution following Prandle (Prandle 1982a), while making a few simplifications based on the description in de Boer (de Boer, Pietrzak and Winterwerp 2006).

The first simplification made is dropping all nonlinear terms. Also, the pressure term is expressed as the change of water level ζ. Equations 1.2 and 1.3 turn into equations 2.2 and 2.3 after simplifications:

$$\begin{cases} equation\ 2: & \frac{\partial u}{\partial t} - fv = -\mathrm{g}\frac{\partial \zeta}{\partial x} + \frac{\partial}{\partial z}\left(E\frac{\partial u}{\partial z}\right) \\ equation\ 3: & \frac{\partial v}{\partial t} + fu = -\mathrm{g}\frac{\partial \zeta}{\partial y} + \frac{\partial}{\partial z}\left(E\frac{\partial v}{\partial z}\right) \end{cases} \quad [2]$$

The boundary conditions can be specified along the vertical z-axis. At the surface ($z = 0$), there is nothing influencing the horizontal velocities. This means that the influence of wind and waves is neglected:

$$z = 0: \quad \frac{\partial u}{\partial z} = 0, \quad \frac{\partial v}{\partial z} = 0 \quad [3]$$

While at the bottom ($z = -D$), a linearised bottom friction $s = \frac{8}{3\pi}\frac{kU}{E}$ acts, where k is a friction factor introduced by Prandle, U is the depth-averaged velocity and E is the eddy viscosity coefficient, which is constant over the entire depth. This results in the following boundary conditions:

$$z = -D: \quad \frac{\partial u}{\partial z} = su, \quad \frac{\partial v}{\partial z} = sv \quad [4]$$

The system of equations can be solved for the velocities u and v by introducing a complex vector notation, where x is the real axis and y is the complex axis. The velocity vector can then be written as $\boldsymbol{U} = u + iv$. For the derivation of the solution and some related properties, read appendix B: Derivation of the analytic solution, as here only the result has been presented.

The velocity vector can be rewritten in terms of an anti-clockwise rotating vector of constant amplitude $\boldsymbol{R}^+$ and a clockwise rotating vector of constant amplitude $\boldsymbol{R}^-$, leading to $\boldsymbol{U} = \boldsymbol{R} = \boldsymbol{R}^+ + \boldsymbol{R}^-$. After some mathematical work we can find a solution for $\boldsymbol{R}^+$ and $\boldsymbol{R}^-$.

$$\frac{\boldsymbol{R}^{\pm}}{\langle \boldsymbol{R}^{\pm} \rangle} = \frac{\cosh\left(\boldsymbol{\alpha}^{\pm}(z-D)\right) - \cos\left(\boldsymbol{\alpha}^{\pm}D\right) - \frac{\boldsymbol{\alpha}^{\pm}}{s}\sinh(\boldsymbol{\alpha}^{\pm}D)}{-\cos(\boldsymbol{\alpha}^{\pm}D) + \left(\frac{1}{\boldsymbol{\alpha}^{\pm}D} - \frac{\boldsymbol{\alpha}^{\pm}}{s}\right)\sinh(\boldsymbol{\alpha}^{\pm}D)} \quad [5]$$

Here $\langle \boldsymbol{U} \rangle$ is the depth-averaged velocity and $\boldsymbol{\alpha}^{\pm}$ is the inverse of the boundary layer height $\boldsymbol{\delta}^{\pm}$:

$$\boldsymbol{\alpha}^{\pm} = (1+i)\sqrt{\frac{f \pm \omega}{2E}} = \frac{1}{\boldsymbol{\delta}^{\pm}} \quad [6]$$

This solution is one of the methods used in the Matlab function Prandle_1982 (see appendix C) as will be covered in the next chapter.

2.3 RHINE ROFI

This property of the velocity vector, writing it as the sum of two counter rotating vectors, can be applied to the vertical structure of the tidal currents in the Rhine ROFI. As mentioned in the introduction, the currents in the Rhine ROFI show entirely different behaviour for neap and spring tides. During neap tide, the water column becomes stratified, the tidal motion becomes elliptic. But during spring tide, the water column is well mixed over the entire vertical and the tidal motion becomes rectilinear again, see Figure 1. This behaviour was also observed in field measurements (Simpson, et al. 1993) and in the outcome of numerical models (de Boer, Pietrzak and Winterwerp 2006). This behaviour can now be explained using the phasors.

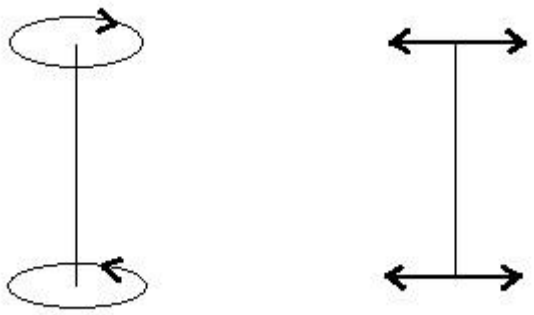

FIGURE 1: DIFFERENT BEHAVIOUR FOR SPRING AND NEAP TIDE: COUNTER ROTATING ELLIPSES (NEAP TIDE) AND RECTILINEAR MOTION (SPRING TIDE).

A water mass flowing over the sea bottom encounters bottom friction. Separating the velocity vector into the two phasors, makes that both phasors will be affected by the bottom friction. They will not be equally affected, because of Earth's rotation. The phasor rotating in the same direction as the Earth (anti-clockwise), $\boldsymbol{R}^{+}$, will experience less friction than the phasor rotating in the opposite direction, $\boldsymbol{R}^{-}$. This has also consequences for the thickness of the boundary layer, for $\boldsymbol{R}^{-}$ the boundary layer will occupy the entire depth, while the boundary layer of $\boldsymbol{R}^{+}$ doesn't even reach half way the vertical. But if the water column becomes stratified, the stratification will shut down turbulence. The upper part is no longer under influence of the bottom friction, but it will now be under influence of the boundary layer between the strata. This is the reason why the behaviour between neap and spring tide is so different: the difference in depth-averaged velocity is such that stratification occurs, shutting down the turbulence and creating the elliptic motion.

3. METHOD

In this project, the analytic solution of Prandle (see previous chapter) has been chosen. This analytic solution has been used for an analytic Matlab model, written by de Boer. This Matlab model is discussed in appendix C.

However, for this investigation the vertical velocity profile during a tidal cycle is required, but this is not the direct outcome of the Matlab model. The next paragraphs will explain how such outcome is obtained. First a vertical velocity profile over the entire depth needs to be obtained. And then the tide needs to be integrated in the model, in order to reach the required outcome: the vertical velocity profile over a tidal cycle.

3.1 USING PRANDLE_1982 TO OBTAIN VELOCITY PROFILES

Prandle_1982 does not give the normalised velocity as direct outcome, but instead it provides one of the two phasors the velocity vector is composed of. The normalised velocity is the sum of two outcomes of Prandle_1982, the positive phasor and the negative phasor. Obtaining a vertical velocity profile is done by dividing the vertical in a discrete set of heights, and using the Matlab function Prandle_1982 to calculate the normalised velocity at each height.

These velocities at different heights are then combined in one plot, which is done for different input values in the next figures. Figure 2 depicts the normalised magnitude profile. The horizontal axis represents the normalised magnitude $U0 = |U|/U_{depthavg}$, the vertical axis the normalised depth $\frac{z}{D}$, where 0 represents the bed and 1 the surface. For the three plots all input parameters have been kept constant, except for k, the friction constant, which is smallest in the leftmost plot, and largest in the rightmost plot. In other words, from left to right the friction increases.

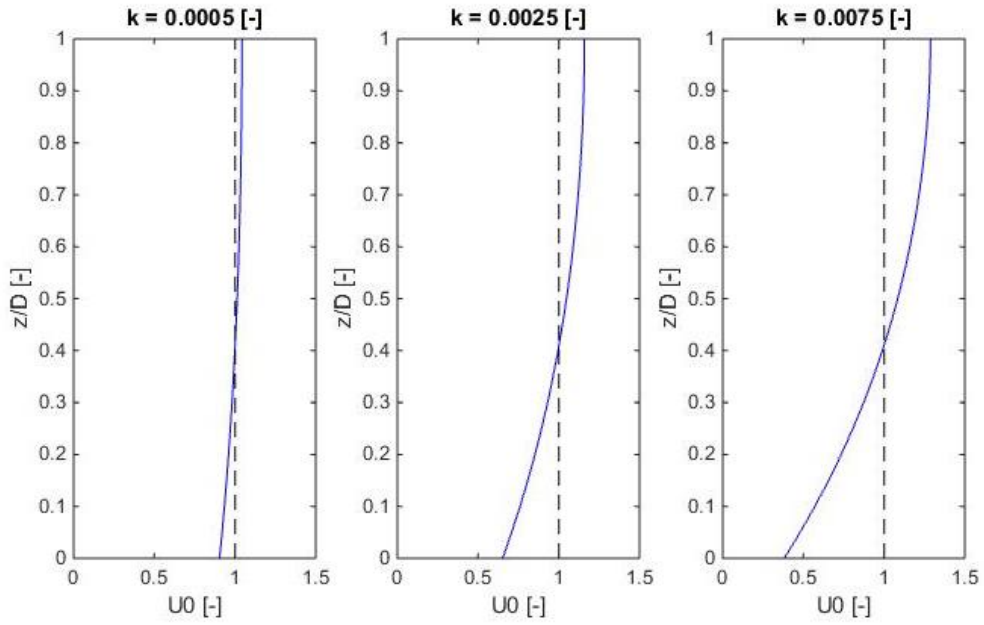

FIGURE 2: AMPLITUDE STRUCTURE FOR INCREASING BOTTOM FRICTION.

The same is done for the phase structure in Figure 3. The horizontal axis represents the phase difference, the angle between the alongshore axis and the direction of the tidal velocity. The vertical axis represents the normalised depth $\frac{z}{D}$. Again, the friction constant k is increasing from left to right, with the same values as in Figure 2, so the phase profile of the leftmost plot of Figure 3 is corresponding to the amplitude structure of the leftmost plot of Figure 2.

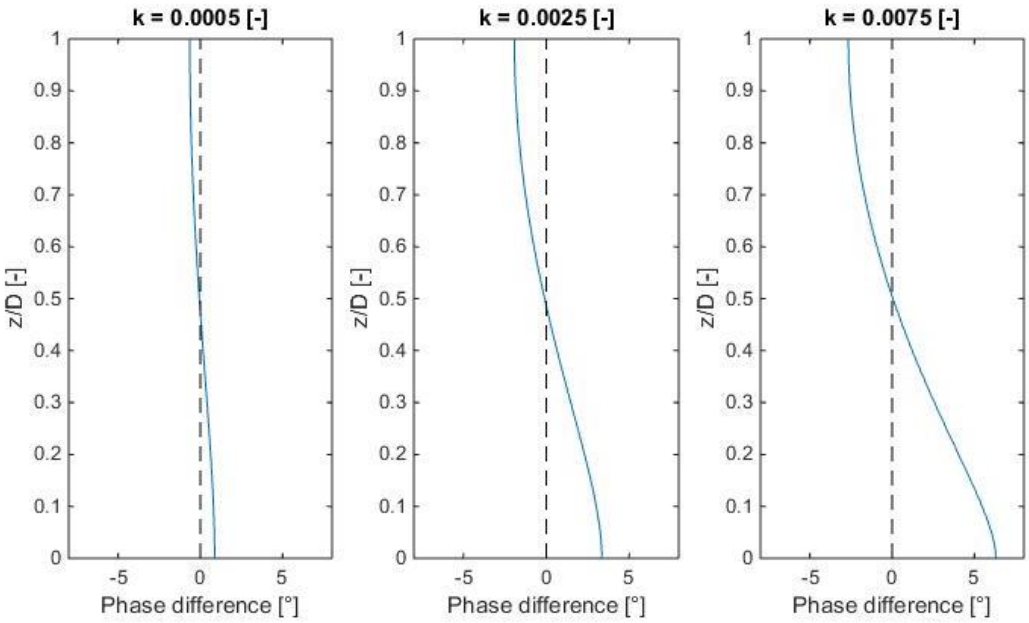

FIGURE 3: PHASE STRUCTURE FOR INCREASING BOTTOM FRICTION.

The easy plots in Figure 2 and Figure 3 indeed correspond to Figure 3 of (Prandle 1982b). This gives an indication of the correct use of Prandle_1982.

3.2 MODELLING THE TIDAL MOTION

The next step is to model the tidal motion. The tide is an oscillatory phenomenon with a period T. So if the tidal motion is split up into two counter rotating phasors, it takes one period for both phasors to make one rotation of 360°, where the positive phasor rotates anticlockwise and the negative clockwise. If ω represents the tidal frequency, the rotating phasors can be defined as $R^+ * e^{i\omega t}$ and $R^- * e^{-i\omega t}$.

This property of the tidal motion is demonstrated in Figure 4. At three instants during a period both phasors, and the resulting tidal vector, are plotted, together with the path they follow over the entire tidal period T. For both phasors, this path is circular. The form of the resulting tidal vector path depends on the rate of both phasors. Most of the time this is elliptic, but if both phasors have the same amplitude, the tidal vector path becomes a straight line, and if one phasor were zero, the tidal vector path would become a circle.

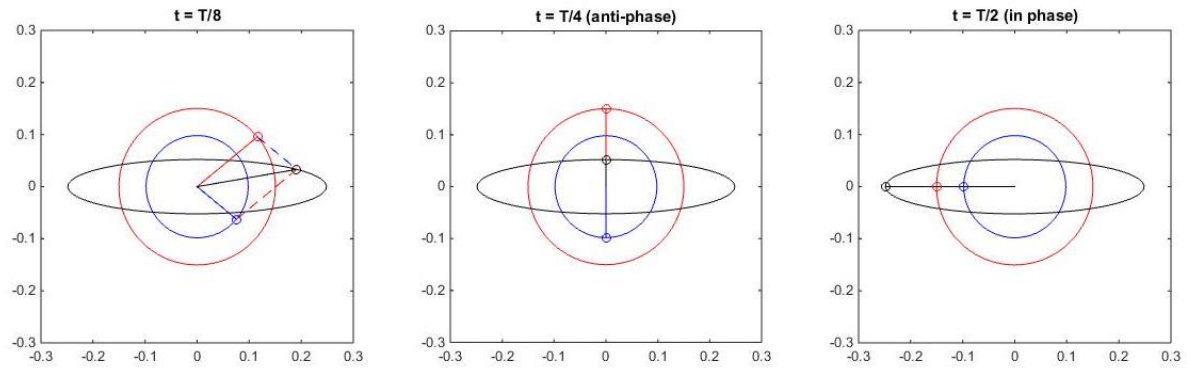

FIGURE 4: TIDAL MOTION SPLIT UP IN PHASORS. R+ IS RED, R- IS BLUE AND U IS BLACK.

The first plot of Figure 4 gives the tidal motion at some random instant, clearly showing how U is the sum of both phasors, while both phasors have opposite phase. The second plot shows the instant when the phasors are in anti-phase, and the third plot when they are in phase.

3.3 USING PRANDLE_1982 TO MODEL VELOCITY PROFILES OVER ENTIRE TIDAL CYCLE

The last step is to include the tidal motion in the vertical profiles, so that the vertical profile over an entire tidal cycle is the outcome. The vertical velocity profile shows the velocity profile at a fixed time instant for the entire depth, while the plot of the tidal motion shows the velocity profile at a fixed height for the entire tidal period. Combining both gives a rotating 3D vertical profile.

Figure 5 shows the rotating vertical profile at three different instants. The velocity profile for U is the sum of two runs of Prandle_1982, one giving the positive phasor, and one giving the negative phasor. This is illustrated in the plots by showing not only the velocity profile for U (in black), but also showing both phasors, R^+ in red rotating anti-clockwise and R^- in blue rotating clockwise. On the left back wall the vertical profile of the cross-shore component at that instant is shown, on the right back wall the vertical profile of the alongshore component.

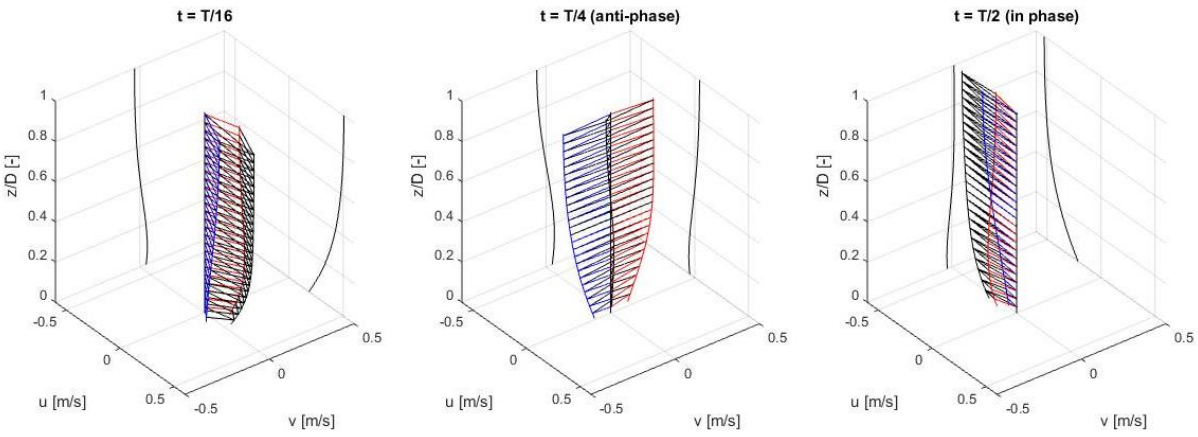

FIGURE 5: VERTICAL PROFILE OF TIDAL MOTION SPLIT UP INTO TWO PHASORS. U IS IN BLACK, R+ IN RED AND R- IN BLUE.

3.4 Comparison Rhine and Fraser river

In order to explore the influence of depth on the behaviour in a ROFI, two cases are compared, the Rhine and the Fraser. In the next table, characteristics of both rivers are given.

	Rhine	Fraser
Depth	20 m	150 m
Depth-averaged velocity	0.6 m/s	0.6 m/s
Tidal frequency	1.4544e-04 rad/s	1.4544e-04 rad/s
Friction constant	0.0025	0.0025
Coriolis parameter	1.1493e-04 rad/s	1.1493e-04 rad/s
Eddy viscosity coefficient	0.0010 – 0.0015	

Table 1: Input parameters for Prandle_1982 for both Rhine and Fraser.

These values will be used in the next chapter. The values have been obtained by making a few simplifying assumptions. The tidal characteristics in the Strait of Georgia are similar to those in the North Sea. Therefore, small differences in tidal characteristics have been neglected[1]. The Coriolis parameter f depends on the latitude, which is 52° for the Rhine, but 49° for the Fraser River. This is a small difference, resulting in a slightly smaller value for f (less than 5% difference), and therefore it will be neglected, assuming f to be the same for both ROFI's. The value for the eddy viscosity coefficient at the Rhine was taken from de Boer (de Boer, Pietrzak and Winterwerp 2006), but no such value could be found for the Fraser. The eddy viscosity coefficient is an important parameter, having a big influence on the behaviour in the ROFI. The process of estimating a value for the Fraser river is outlined in the next paragraph.

3.5 Estimating the eddy viscosity

The eddy viscosity is used for modelling the complicated phenomenon of turbulence. To have a clear view on the influence of the eddy viscosity coefficient E on the velocity profile, see appendix D. It is clear that a small change in E can have a big impact, and therefore the choice for the value of E will be crucial.

The most important assumption in this model, and also a big restriction of the model, is the assumption of a constant eddy viscosity coefficient E over the entire depth. As a first approach, a definition presented by Prandle (Prandle 1982b) based on a formulation by Bowden (Bowden 1953), was used to define a relationship between the eddy viscosity coefficient and the depth: $E = \alpha * U_{depthavg} * D$. This alpha is a dimensionless constant, for which the value has been determined for the Rhine: $\alpha = 0.0012$ (de Boer, Pietrzak and Winterwerp 2006). This value was found by calibrating the model to numerous measurements[2].

This definition means that the eddy viscosity coefficient increases with depth. But is this realistic? The eddy viscosity is used to model turbulence. This turbulence is mainly caused near the boundaries of our domain, through bottom friction at the bed and for example wind friction at the surface (although in this approach all friction at the surface is neglected). For larger depths, the influence zone where the bed friction acts becomes relatively smaller. So, taken over the entire depth, there

[1] More information on the tide in the Strait of Georgia can be found in Foreman (Foreman, et al. 1995).
[2] For observations and comparison between measurements and models see Simpson (Simpson, et al. 1993).

will be less turbulence, which has to be modeled using a smaller eddy viscosity coefficient E. It would be even more precise if the value of E could differ over depth, using a larger value near the boundary and a smaller value in the upper part where there is nearly no mixing caused by turbulence. But, expecting E to decrease with depth is not in line with Bowden's formula. Therefore it might be useful to define an inverse relation between E and D for which E decreases when D increases.

For this analysis two different relations between E and D will be used. The first relation is the one presented by Bowden, for which $E \sim D$: $E_1 = \alpha * U_{depthavg} * D$. This relation was based on Buckingham's pi theorem, in order to come up with a dimensionally consistent formulation, so that the coefficient α is dimensionless. For the second relation an equation is required such that E decreases when the depth increases, for example $E \sim {}^{1}/_{D}$. An expression similar to Bowden's equation has been chosen here, but instead of multiplying with depth, dividing by depth. This gives the following equation: $E_2 = \beta * U_{depthavg}/D$. It is unknown whether this equation gives correct values for E, but it does give an idea of the behaviour for smaller E's. The coefficient β is chosen such that for the situation at the Rhine ROFI, so for $D = 20m$, the eddy viscosity coefficient E is the same for both relations. This gives $\beta = \alpha * {D_{Rhine}}^2 = 0.0012 * (20m)^2 = 0.48m^2$. Note that, in contrast to α, β is not a dimensionless parameter. Therefore, the depth should always be given in meters and the depth-averaged velocity in meters per second. Both relations are shown in the next plot, and it can be concluded that the second relation exhibits the desired behaviour, decreasing for increasing depth.

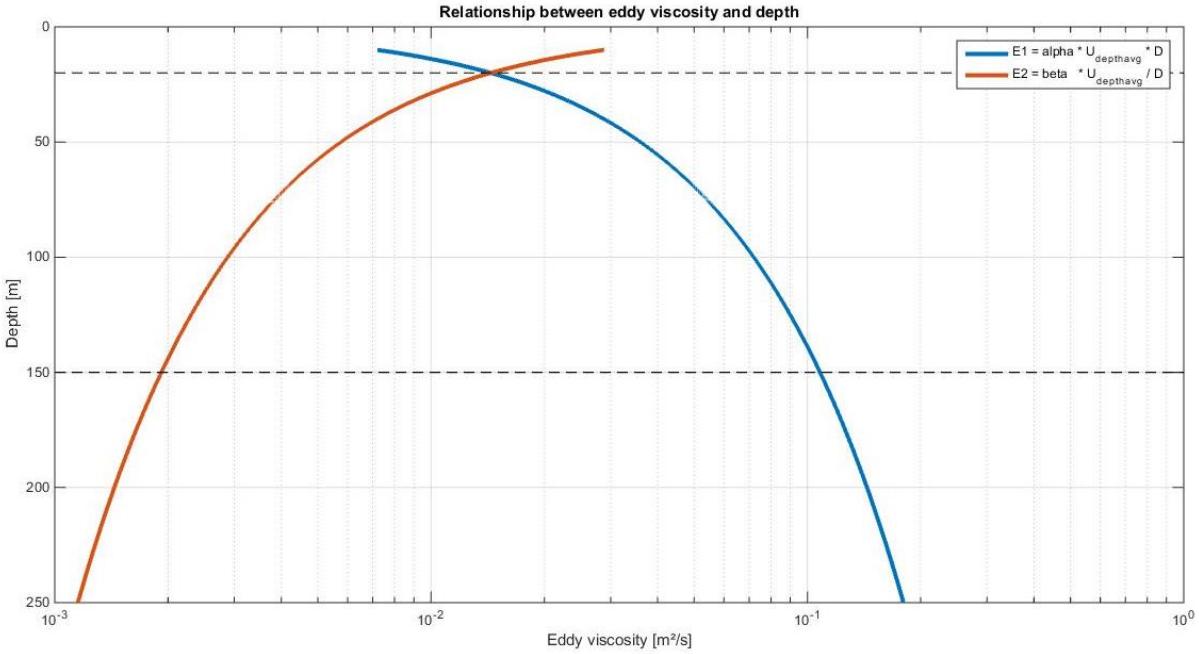

FIGURE 6: RELATIONSHIP BETWEEN EDDY VISCOSITY AND DEPTH. BOWDEN'S EQUATION FOR E1 IN BLUE, THE INVERSE EQUATION FOR E2 IN ORANGE.

4. RESULTS

All the necessary information has been gathered to finally look into what will happen if this model is applied to a river discharging into a deeper sea. In this particular case, the Rhine will be compared with the Fraser river. From the previous analysis, the only parameters that differ between those two rivers, are the depth and the related eddy viscosity coefficient (for two possible relationships have been defined in the previous chapter). All other input parameters for Prandle_1982 are constant, see Table 1.

4.1 VELOCITY PROFILES FOR BOWDEN'S EDDY VISCOSITY RELATION

Using these values, Prandle_1982 has been used to plot the velocity profile for a range of depths between 10m and 1000m for both eddy viscosity relations. Starting from Bowden's relation for the eddy viscosity: $E_1 = \alpha * U_{depthavg} * D$. This relation gives an eddy viscosity of $E_{1,Rhine} = 0.014\ m^2/s$ for the Rhine and $E_{1,Fraser} = 0.1\, m^2/s$ for the Fraser. Figure 7 shows the amplitude structure for a range of depths, where the horizontal axis represents the range of depths and the vertical axis the normalised depth. The colours represent the amplitude structure, and the two vertical lines indicate the depth for the Rhine and for the Fraser.

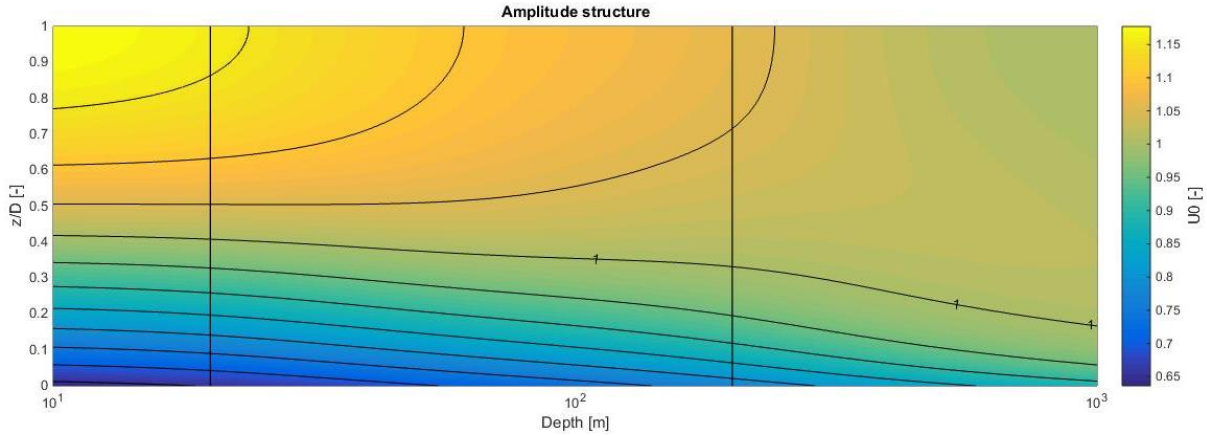

FIGURE 7: AMPLITUDE STRUCTURE FOR A RANGE OF DEPTHS, USING BOWDEN'S RELATION FOR E.

From the above plot, representing the amplitude structure for a range of depths, one can say that for greater depth only in the bottom layers a large velocity gradient occurs, while for the largest, upper part of the water column, the velocity is almost constant over depth. This seems like a realistic behaviour, since for larger depth a smaller fraction of the water column is influenced by the bed friction.

Figure 8 shows the phase structure for a range of depths, where the phase is expressed as the phase difference with respect to the surface layer.

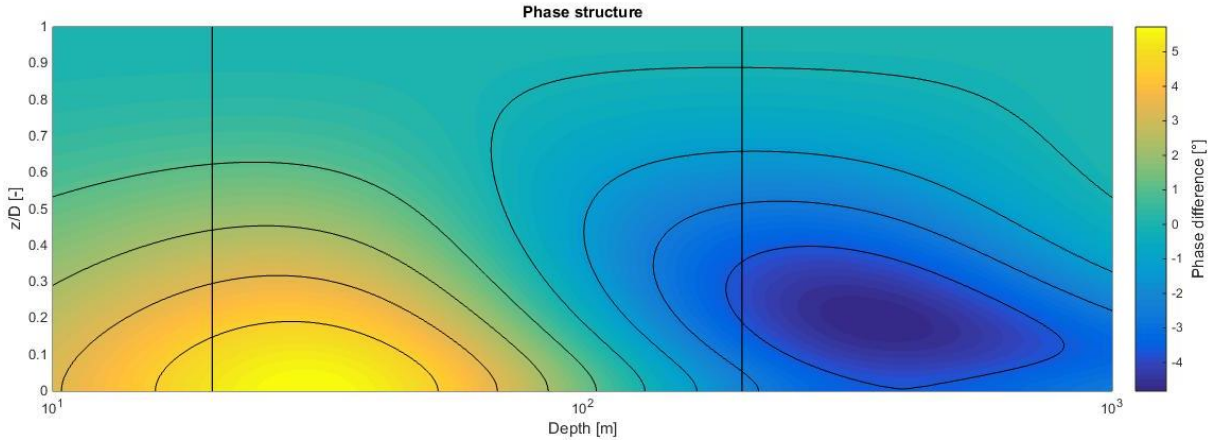

FIGURE 8: PHASE STRUCTURE FOR A RANGE OF DEPTHS, USING BOWDEN'S RELATION FOR E.

This plot indicates that there is a change in behaviour over depth. For smaller depths, the phase at the bed is ahead of the surface, while around a depth of 100m the behaviour shifts into the phase at the surface being ahead.

4.2 VELOCITY PROFILES FOR THE INVERSE EDDY VISCOSITY RELATION

Next is the second relationship for the eddy viscosity coefficient, the inverse relation, $E_2 = \beta * U_{depthavg}/D$, for which E decreases as depth increases. All other input parameters remain the same as used for the plots for Bowden's relation for E. This relation results in the same value for the eddy viscosity coefficient for the Rhine, $E_{2,Rhine} = 0.014\ m^2/s$, but a much smaller eddy viscosity coefficient for the Fraser, $E_{2,Fraser} = 0.001\ m^2/s$. Below, Figure 9 shows the amplitude structure for a range of depths, where the horizontal axis represents the range of depths and the vertical axis the normalised depth. The colours represent the amplitude structure, and the two vertical lines indicate the depth for the Rhine and for the Fraser.

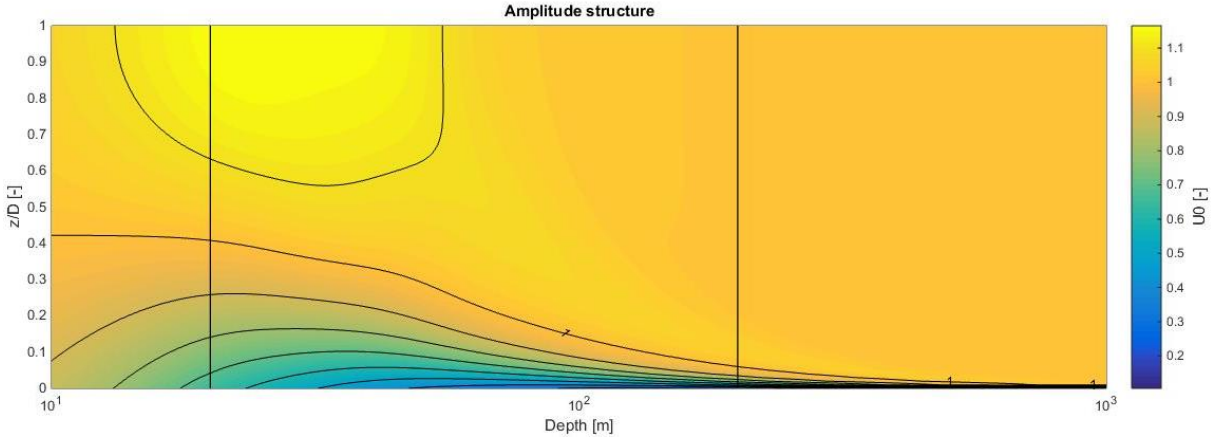

FIGURE 9: AMPLITUDE STRUCTURE FOR A RANGE OF DEPTHS, USING THE INVERSE RELATION FOR E.

From the above plot, representing the amplitude structure for a range of depths, similar behaviour as for Bowden's relation for E is observed. For larger depth only in the bottom layers a large velocity gradient occurs, while for the largest, upper part of the water column, the velocity is constant over depth. The bottom layer is much smaller than for Bowden's relation. This seems like a realistic

behaviour, since for larger depth a smaller fraction of the water column is influenced by the bed friction. Figure 10 shows the phase structure for a range of depths for our inverse relation for E.

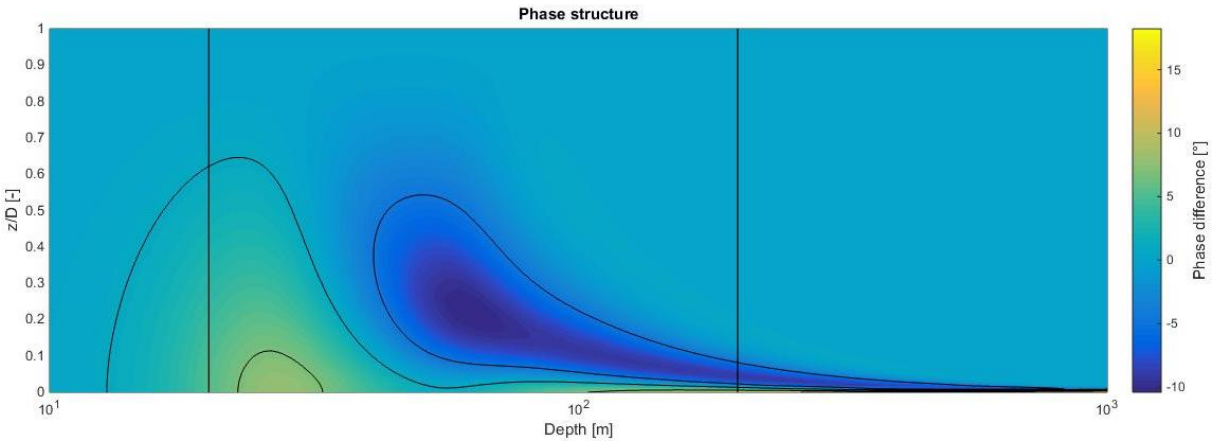

FIGURE 10: PHASE STRUCTURE FOR A RANGE OF DEPTHS, USING THE INVERSE RELATION FOR E.

This plot gives a different image from the plot of the phase structure for Bowden's relation. The biggest difference is the size of the phase differences, which is three times as large here, compared to the phase differences for Bowden. This is a consequence of the smaller eddy viscosities, since, as shown in appendix D, the phase differences become larger for smaller eddy viscosities, since smaller eddy viscosities represent less turbulence or less mixing. But, at closer inspection, there are also similarities between the phase structures of both eddy viscosity relations. In the shallow zone, the phase difference is focused in the lower half of the water column, with the phase at the bottom being ahead of the phase at the surface. At larger depth, for a layer above the bottom layer, the phase lags behind the phase at the surface.

4.3 COMPARISON VELOCITY PROFILES FOR RHINE AND FRASER

Figure 11 shows, from left to right, the amplitude structure at the Rhine ROFI (which is the same for both eddy viscosity relations), and the amplitude structure at the Fraser ROFI for the two eddy viscosity relations.

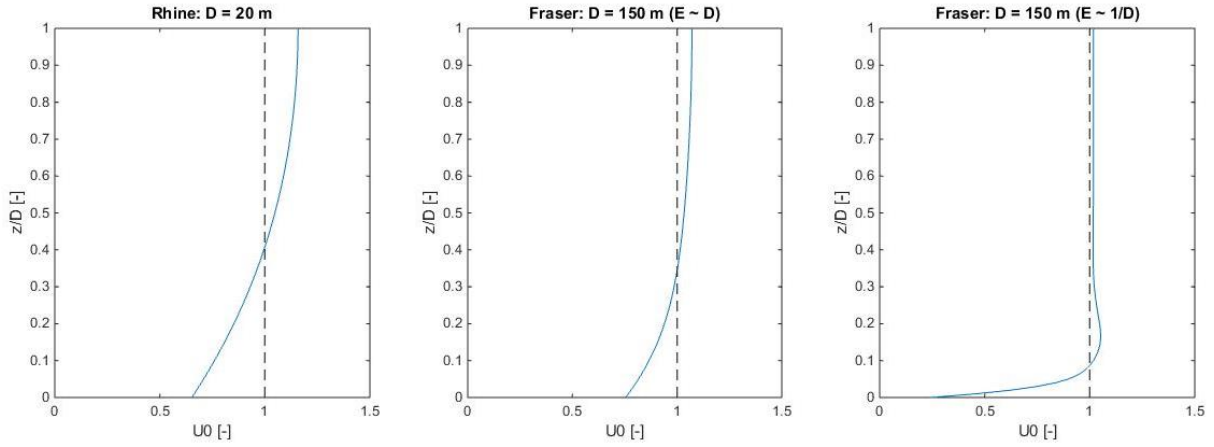

FIGURE 11: AMPLITUDE STRUCTURE FOR THE RHINE (LEFT) AND THE FRASER (MIDDLE FOR E ~ D, RIGHT FOR E ~ 1/D).

A first observation shows that for the Rhine more than half of the water column is influenced by the bed friction, while for the Fraser, for both eddy viscosity relations, a smaller fraction of the water column is influenced. This is the expected behaviour, showing the difference between the shallow and deep situations. Second, when looking at the two plots for the Fraser, the size of the boundary layer differs, being smaller for the inverse relation for E. Additionally, for Bowden's relation, there is still a small gradient in the amplitude structure for the upper part of the water column, while for the inverse relation, the amplitude is constant over the entire upper part. This last behaviour means that the upper part of the water column moves as a rigid block, while the entire turbulence and mixing takes place in the small bottom layer where the bed friction acts.

For the amplitude structure, it seems like the inverse relation for E gives a more realistic result. But this amplitude structure shows only one component of the velocity profile. As such, for a complete analysis, the phase structures need to be compared as well. These phase structures are given in Figure 12, which shows, from left to right, the phase structure at the Rhine ROFI (which is the same for both eddy viscosity relations), and the phase structure at the Fraser ROFI for the two eddy viscosity relations. Again, the phase structure is plotted as the difference with the phase at the surface.

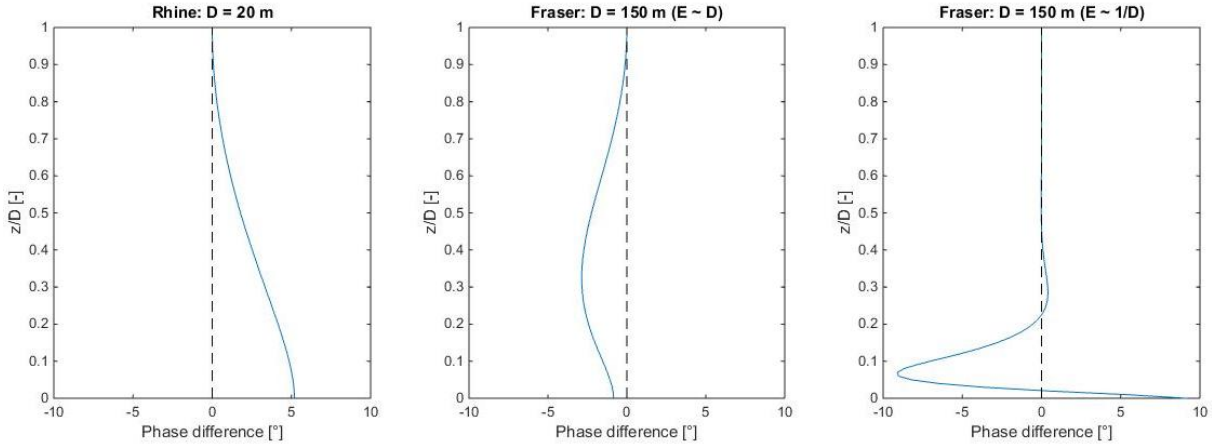

FIGURE 12: PHASE STRUCTURE FOR THE RHINE (LEFT) AND THE FRASER (MIDDLE FOR E ~ D, RIGHT FOR E ~ 1/D).

The left plot, depicting the phase structure for the Rhine, shows that the phase difference increases downwards, with a maximum near the bed of 5°, the phase at the bed being ahead of the surface. The middle plot, depicting the phase structure for the Fraser for Bowden's eddy viscosity relation, shows only small phase differences, reaching a maximum somewhere under the middle of the water column of 3°, the phase lagging behind the phase at the surface. As a result of this, and related to the inverse eddy viscosity relation, two big differences are apparent. First of all, the phase differences are much bigger, reaching almost 10°, and second, the zone containing the phase differences is a small boundary layer near the bed, with the upper part of this layer having negative phases (so lagging behind) and the lower part having positive phases. The upper part of the vertical column has no phase difference with the surface. This contributes to the theory that for large depths, the upper part of the water column moves as a rigid block, while all mixing takes place in the lower boundary layer.

After comparing the results of both depth – eddy viscosity relations for the Fraser river with the Rhine, it looks like Bowden's relation gives more of a scaled version of the shallow water situation, while the inverse relation gives a better representation of the deep situation, with the upper part behaving as a rigid block.

4.4 Comparison spring and neap tide Fraser

For the Rhine there is also a big difference in the behaviour for spring and neap tides (see appendix D). Therefore it might be useful to have a look at the spring/neap behaviour of the Fraser ROFI. So far, a depth-averaged velocity of $U_{depthavg} = 0.6\,{}^{m}/_{S}$ has been used. To simulate spring/neap behaviour, two different depth-averaged velocities will be applied, one representing neap tide, $U_{neap} = 0.43\,{}^{m}/_{S}$, and one representing spring tide, $U_{spring} = 0.66\,{}^{m}/_{S}$. Also the eddy viscosity coefficient will be different for spring and neap tide, since it is dependent on the depth-averaged velocity.

Figure 13 shows the elliptic profiles for spring tide (upper row) and neap tide (lower row). For these plots, the inverse eddy viscosity relation has been used.

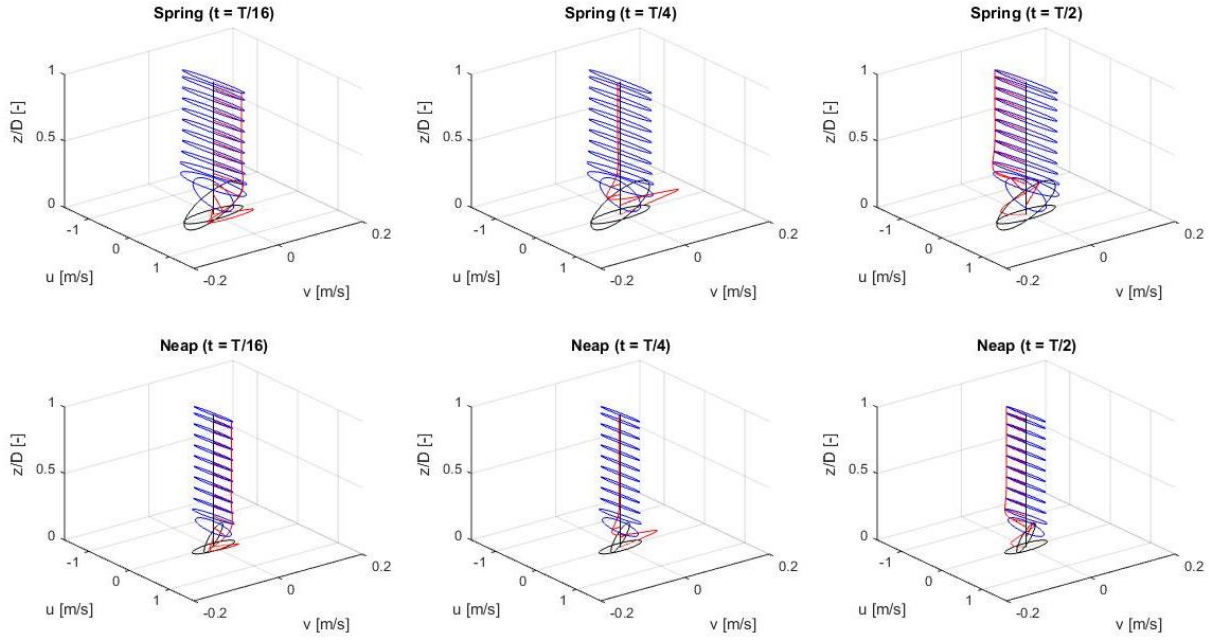

Figure 13: Elliptic profiles for the Fraser river at different times during a tidal cycle. Upper row represents spring tide, lower row represents neap tide.

From these plots one can conclude that for both neap and spring tide, for the largest part of the water column, the tidal motion is rectilinear. Only in a small boundary layer the velocity profile behaves differently, with higher ellipticity and counter rotating ellipses. For spring tide these differences are larger, which is caused by higher velocities. But, in contrast to the Rhine, there is no big difference in behaviour between neap tide and spring tide in case of the Fraser.

5. CONCLUSIONS AND RECOMMENDATIONS

Rivers, like the Rhine and the Fraser, discharging their fresh water into a salty sea, have a big impact on the currents in a large zone around the mouth of the river, the zone also known as the region of fresh water influence. The density differences influence the existing tidal motion in the coastal sea in a complex interaction.

5.1 CONCLUSIONS

The first goal of this project was to understand the complex behaviour of the tidal velocity profile in the Rhine ROFI, for which this model was built. This has been done by deriving the governing equations and an analytic solution, and by using the Matlab function Prandle_1982 for various sets of input parameters. Without a fresh water discharge, the tidal motion in the North Sea would be rectilinear, parallel to the coastline, having a regular vertical profile. But with the fresh water discharge from the Rhine, the behaviour in the Rhine ROFI becomes very different.

On top of this, the difference between the depth-averaged velocity at spring tide and at neap tide crosses a critical limit, which results in different characteristics of the ROFI for spring and neap tides. During neap tide, the water column stratifies, which reduces the mixing between fresh water from the Rhine and salt water from the North Sea, and the tidal motion becomes elliptic, showing strong cross-shore components of the current. But during spring tide, the depth-averaged velocity is high enough to mix the entire water column, cancelling the stratification, and the tidal motion becomes rectilinear again.

Besides the depth-averaged velocity, another parameter also plays an important role in modelling this behaviour: the eddy viscosity. This eddy viscosity coefficient E is used to model the very complex phenomenon of turbulence. In this case, the neap tide, characterised by stratification which reduces the turbulence, is modelled using a lower value for E than for spring tide, when more turbulence occurs.

The second goal, and main objective of this project, was to investigate the influence of the depth on the behaviour of the tidal velocity profile in the region of fresh water influence. This investigation was done by comparing the Rhine with the Fraser, where the main difference between both ROFI's is the depth, 20m for the Rhine against 150m for the Fraser.

The biggest issue in this investigation turned out to be finding realistic values for the eddy viscosity coefficient for the Fraser ROFI. For the Rhine, numerous field measurements and a validated numerical model have provided a range of realistic values for E. Without these field data or some numerical model for the Fraser, it is almost impossible to find representative values for the eddy viscosity coefficient. Therefore the only option to assess a representative range was to use approximating equations, relating the eddy viscosity coefficient to the depth. One such equation was presented by Bowden, and using the field data and the numerical model, values for the dimensionless constant defining this relationship for the Rhine ROFI have been determined. Using Bowden's equation, a first approximation for the eddy viscosity coefficient in the Fraser ROFI could be made.

Since $E \sim D$ for this relationship, this resulted in a much bigger value for E at the Fraser ROFI. For such a large depth, the assumption for a constant eddy viscosity over the entire depth becomes almost untenable. For large depths, there is actually almost no mixing over the largest part of the vertical, the mixing being concentrated near the boundaries. This means that the large upper part of the water column should be represented with a very small value for E, while the small boundary layer requires a larger value. Finding a representative constant value for E means a small value must be chosen. An inverse relation between the eddy viscosity and the depth therefore seems more appropriate, for example $E \sim {}^{1}/_{D}$. Such an equation was also tested and this resulted in possible realistic velocity profiles, showing the upper part of the water column behaving more or less like a rigid block, while the mixing takes place near the bottom layer.

For fresh water flowing in near the surface, this means at large depth that the river plume would undergo less mixing, with most turbulence near the bottom and some turbulence at the fresh/salt interface.

This analytic model has proven to be a good tool to gain insight in the influence of depth on the behaviour of ROFI's. In shallow situations, the bottom friction influences the entire vertical, while in very deep situations, the largest upper part of the vertical behaves as a rigid block, all turbulence taking place in a small boundary layer near the bottom. However, due to the numerous simplifications and assumptions, this model cannot be used for prediction.

5.2 Recommendations

To model ROFI's in very deep coastal seas, such as the Strait of Georgia, this analytic model based on Prandle, is not very appropriate for prediction, due to the assumption of a constant eddy viscosity coefficient over the entire depth.

Actually such an assumption is never realistic, but for the Rhine ROFI it was possible to find a value for E through calibrating the model results with the measurements. So if this model is applied to a different ROFI, widespread measurements of the situation at that ROFI are required, in order to find out whether there exists some value for E such that the model fairly represents the real behaviour. The approximating depth – eddy viscosity relations remain to be proven, even the existence of such relation. Only if for numerous ROFI's realistic values for E have been found, such a relation may be derived (if it exists).

A better way to model the eddy viscosity in case of stratification is to leave the assumption of a constant eddy viscosity coefficient over the entire depth. For example, a different formulation for the eddy viscosity was presented by Howarth (Howarth 1998). He divides the depth into a few layers, and for each layer he takes a linearly changing eddy viscosity. Using this assumption, a new analytic solution can be derived for each layer, and boundary conditions must provide continuity over the layer boundaries. This method is also only possible if there is an extensive data set of measurements, to compare the approximate piecewise linear eddy viscosity with the real situation. It still remains an approximation, but it does take into account some effects of stratification.

In any case, field data are necessary to develop a model of a ROFI. Using the assumption of a constant eddy viscosity over the entire depth gives an easier solution, but a piecewise linear eddy viscosity will represent the effects of stratification more accurately.

6. EPILOGUE AND ACKNOWLEDGEMENTS

The Bachelor thesis is the last element of my Bachelor degree in Civil Engineering. It bridges Bachelor and Master, challenges the knowledge and skills acquired over the past three years in order to show the ability to think and work independently. This project is my very first project that requires to work individually and, although under guidance of prof. Pietrzak, to show my capability to think and make reflections in an independent way, which is not easy. Gaining understanding in such a specific, complicated problem as ROFI's has turned out to be quite a challenge.

The first step was to study existing papers on the subject, but without any foreknowledge in Oceanography, understanding even the basics or getting familiar with the topic proved to be quite challenging. But after a couple of weeks of hard working I finally got a grip on the subject, ready to start exploring the Matlab model.

Once there, unfortunately I became ill, being absent for more than a month and not able to continue working on this project. Luckily I have been given the possibility to finish my project during the summer break, and for this I would like to thank the university for being so flexible, Dr. ir. Astrid Blom for being so involved and making it possible for me to finish my project after all, and Prof. dr. Julie Pietrzak for guiding me, even during the holidays.

Once recovered, I resumed my project where I left off, starting to explore the Matlab model. It took me again some time to understand how the model worked and how to use it and so I was finally ready to dig into the main research question. I would like to thank Ir. Gerben de Boer for his help with the Matlab model he wrote himself and Ir. Sabine Rijnsburger for her new ideas whenever I got stuck, and especially for her help with the finishing touch of the report. It needs to be said that without my Minor in Applied Mathematics at Virginia Tech last Fall semester I would not have had the necessary skills and knowledge to work with Matlab for this project.

This report presents the result of my work. At first sight it might be less than the result I expected when I started this project, slightly underestimating this very complex subject. But after the past three months and knowing much more on the subject matter, I realise that my expectations weren't realistic at all. Understanding and absorbing this complex and new domain on my own, and writing and running scripts for Matlab, is an achievement to really be proud of, which I am.

Thank you for reading, and I hope you've enjoyed the same, satisfying, feeling you get when you "see the light", finally getting the hang of it.

Silke Tas

Delft, July 2014

7. REFERENCES

7.1 CONSULTED SOURCES

Bowden, K. F. “Note on wind drift in a channel in the presence of tidal currents.” *Proceedings of the Royal Society of London* (cited by Prandle), 1953: 426-446.

de Boer, G. J., J. D. Pietrzak, and J. C. Winterwerp. “On the vertical structure of the Rhine region of freshwater influence.” *Ocean dynamics*, 2006: 198-216.

Foreman, M. G. G., R. A. Walters, R. F. Henry, C. P. Keller, and A. G. Dolling. “A tidal model for eastern Juan de Fuca Strait and the southern Strait of Georgia.” *Journal of Geophysical Research*, 1995: 721-740.

Gill, A. E. *Atmosphere-Ocean Dynamics.* London: Academic Press, 1982.

Howarth, M. J. “The effect of stratification on tidal current profiles.” *Continental Shelf Research*, 1998: 1235-1254.

Huthnance, J. M. “The PROFILE project: an overview.” *Journal of Marine Systems*, 1997: 249-261.

Pietrzak, J. D. *An introduction to oceanography for civil and offshore engineers.* Delft: TU Delft, 2014.

Prandle, D. “The vertical structure of tidal currents.” *Geophysical & astrophysical fluid dynamics*, 1982b: 29-49.

Prandle, D. “The vertical structure of tidal currents and other oscillatory flows.” *Continental Shelf Research*, 1982a: 191-207.

Simmon, R., and J. Allen. *NASA Earth Observatory.* 7 September 2011. http://earthobservatory.nasa.gov/IOTD/view.php?id=77368&src=eorss-iotd (accessed July 2014).

Simpson, J. H., et al. “Periodic stratification in the Rhine ROFI in the North Sea.” *Oceanol Acta*, 1993: 23-32.

7.2 List of images

APPENDICES

A. DERIVATION OF THE SYSTEM OF EQUATIONS

In this appendix the six equations used for modelling the Rhine ROFI will be derived. But the concept of the total derivative needs to be introduced. After that, the six equations are derived along the description in the lecture notes of "An introduction to oceanography for civil and offshore engineers" (Pietrzak 2014).

A.1 TOTAL DERIVATIVE

This explanation of the total derivative follows the Gill's (Gill 1982). The total derivative is the rate of change of a physical quantity that is subjected to a velocity field. This physical quantity can be anything, and is a function of position $\boldsymbol{X} = (x, y, z)$ and time t. The symbol $\frac{D}{Dt}$ is used for total derivative. Here, the total derivative of some physical quantity $\gamma(x, y, z, t)$ is derived:

$$\frac{D\gamma}{Dt} = \frac{\partial\gamma}{\partial t} + \frac{\partial\gamma}{\partial x}\frac{dx}{dt} + \frac{\partial\gamma}{\partial y}\frac{dy}{dt} + \frac{\partial\gamma}{\partial z}\frac{dz}{dt} = \frac{\partial\gamma}{\partial t} + \frac{\partial\gamma}{\partial x}u + \frac{\partial\gamma}{\partial y}v + \frac{\partial\gamma}{\partial z}w = \frac{\partial\gamma}{\partial t} + \boldsymbol{V}\nabla\gamma \qquad [7]$$

Where $\boldsymbol{V}$ is the velocity vector. Therefore, the symbol $\frac{D}{Dt}$ means:

$$\frac{D}{Dt} = \frac{\partial}{\partial t} + \frac{\partial}{\partial x}u + \frac{\partial}{\partial y}v + \frac{\partial}{\partial z}w \qquad [8]$$

This total derivative can now be used in the derivation of the system of equations.

A.2 CONTINUITY EQUATION

Consider a very small fluid element. On this element a mass balance is applied, which can be written in words as "*rate of increase of mass in fluid element" = "flux of mass into fluid element" – "flux of mass out of fluid element"*. In symbols the resulting mass balance is given by:

$$\frac{\partial\rho}{\partial t} + \frac{\partial(\rho u)}{\partial x} + \frac{\partial(\rho v)}{\partial y} + \frac{\partial(\rho w)}{\partial z} = 0 \qquad [9]$$

For an incompressible fluid, the density is considered a constant, and the continuity equation simplifies to equation 10, which is equation 1.1 in the system of equations describing a ROFI.

$$\frac{\partial u}{\partial x} + \frac{\partial v}{\partial y} + \frac{\partial w}{\partial z} = 0, \ or \qquad \nabla\boldsymbol{V} = 0 \qquad [10]$$

A.3 3D EQUATIONS OF MOTION

To derive the 3D equations of motion, start by applying Newton's second law, "mass" * "acceleration" = "force", to a very small fluid element:

$$\rho dxdydz * \frac{D\boldsymbol{V}}{Dt} = \boldsymbol{F} \quad [11]$$

The right hand side in equation 11, $\boldsymbol{F}$, is the resultant force acting on the element. The different forces exerted on the element are pressure forces, viscous forces and gravitational forces. This last category, the gravitational forces, can be split up into two categories: in vertical direction representing the weight of the small element $\rho g dxdydz$, while in the horizontal directions it is the Coriolis force. This is the effect of Earth's rotation, as a consequence of our assumption that the coordinate system is fixed. We will make another assumption to simplify the Coriolis term, the so called f-plane approximation, where the Coriolis force is assumed to be constant with latitude. The Coriolis parameter f is given by $f = 2 * \Omega * \sin(\varphi)$, where Ω is a constant representing the angular velocity of rotation of the Earth, with $\Omega = \frac{2\pi}{1\ day} = 7.2921 * 10^{-5} \frac{rad}{s}$ and φ is the average latitude of the considered domain (52° for the Rhine ROFI).

This leads to the following system of equation, also known as the Navier-Stokes equations. The right hand side of each equation consists of, respectively, the pressure term, the gravitational term and the viscosity term.

$$\begin{cases} \rho \frac{Du}{Dt} = -\frac{\partial p}{\partial x} + fv + \left[\frac{\partial \tau_{xx}}{\partial x} + \frac{\partial \tau_{yx}}{\partial y} + \frac{\partial \tau_{zx}}{\partial z}\right] \\ \rho \frac{Dv}{Dt} = -\frac{\partial p}{\partial y} - fu + \left[\frac{\partial \tau_{xy}}{\partial x} + \frac{\partial \tau_{yy}}{\partial y} + \frac{\partial \tau_{zy}}{\partial z}\right] \\ \rho \frac{Dw}{Dt} = -\frac{\partial p}{\partial z} - \rho g + \left[\frac{\partial \tau_{xz}}{\partial x} + \frac{\partial \tau_{yz}}{\partial y} + \frac{\partial \tau_{zz}}{\partial z}\right] \end{cases} \quad [12]$$

By making some other assumptions, these equations can be simplified even more. First of all hydrostatic conditions are assumed, which simplifies the equation of motion in z-direction into $\frac{\partial p}{\partial z} = -\rho g$. Since the differences in density are relatively small, the effects of density difference are assumed not to affect the horizontal momentum. Therefore, in the first two equations, describing the horizontal directions, density is assumed constant: ρ_0. This is the so called Boussinesq approximation.

To simplify the viscosity terms, Reynolds turbulence model is applied. By using Reynolds averaging and introducing E as the vertical eddy viscosity coefficient, the viscosity term can be rewritten, for example in x-direction, as $\frac{\partial \tau_{xx}}{\partial x} + \frac{\partial \tau_{yx}}{\partial y} + \frac{\partial \tau_{zx}}{\partial z} \approx -F_x - \frac{\partial}{\partial z}\left(E \frac{\partial u}{\partial z}\right)$, where F_x contains the horizontal terms (which are neglected in our model). These assumptions lead to the 3D equations of motion as presented in the second chapter in equations 1.2, 1.3 and 1.4.

$$\begin{cases} \frac{\partial u}{\partial t} + \frac{\partial u^2}{\partial x} + \frac{\partial uv}{\partial y} + \frac{\partial uw}{\partial z} - fv + \frac{1}{\rho_0}\frac{\partial p}{\partial x} - F_x - \frac{\partial}{\partial z}\left(E\frac{\partial u}{\partial z}\right) = 0 \\ \frac{\partial v}{\partial t} + \frac{\partial vu}{\partial x} + \frac{\partial v^2}{\partial y} + \frac{\partial vw}{\partial z} + fu + \frac{1}{\rho_0}\frac{\partial p}{\partial y} - F_y - \frac{\partial}{\partial z}\left(E\frac{\partial v}{\partial z}\right) = 0 \\ \frac{\partial p}{\partial z} = -\rho g \end{cases} \quad [13]$$

A.4 SALINITY AND HEAT

Using similar assumptions for the conservation equations for salinity and temperature, the last two equations of the system of equations are given underneath. Here, S is the salinity in PSU and T is the temperature in °C. S_{SS} refers to sources and sinks, and Q_H refers to the heat exchange, while D_t is diffusivity coefficient. These two equations form the last two equations in the system of equations [1].

$$\begin{cases} \frac{\partial S}{\partial t} + \frac{\partial uS}{\partial x} + \frac{\partial vS}{\partial y} + \frac{\partial wS}{\partial z} - F_S - \frac{\partial}{\partial z}\left(D_t\frac{\partial S}{\partial z}\right) = S_{SS} \\ \frac{\partial T}{\partial t} + \frac{\partial uT}{\partial x} + \frac{\partial vT}{\partial y} + \frac{\partial wT}{\partial z} - F_T - \frac{\partial}{\partial z}\left(D_t\frac{\partial T}{\partial z}\right) = \frac{1}{\rho}Q_H + S_{SS} \end{cases} \quad [14]$$

Temperature, salinity and pressure are used to calculate the density according to the UNESCO equation of state, see (Gill 1982).

B. Derivation of the analytic solution

B.1 Analytic solution using complex notation

The system of equations can be solved for u and v by introducing a complex vector notation, where x is the real axis and y is the complex axis. The velocity vector can then be written as $\boldsymbol{U} = u + iv$, and u and v can be written as follows, where ω is the angular frequency and a, b, c and d are (unknown) coefficients.

$$\begin{cases} u = a\cos(\omega t) + b\sin(\omega t) = a\frac{e^{i\omega t}+e^{-i\omega t}}{2} + b\frac{e^{i\omega t}-e^{-i\omega t}}{2i} = \frac{1}{2}(a-ib)e^{i\omega t} + \frac{1}{2}(a+ib)e^{-i\omega t} \\ v = c\cos(\omega t) + d\sin(\omega t) = c\frac{e^{i\omega t}+e^{-i\omega t}}{2} + d\frac{e^{i\omega t}-e^{-i\omega t}}{2i} = \frac{1}{2}(c-id)e^{i\omega t} + \frac{1}{2}(c+id)e^{-i\omega t} \end{cases} \quad [15]$$

This way of writing u and v shows that the velocity vector $\boldsymbol{U}$ can be rewritten in terms of an anti-clockwise rotating vector of constant amplitude $\boldsymbol{R}^+$ and a clockwise rotating vector of constant amplitude $\boldsymbol{R}^-$, giving $\boldsymbol{U} = \boldsymbol{R} = \boldsymbol{R}^+ + \boldsymbol{R}^-$. Using the previous equations for u and v, the following equations for $\boldsymbol{R}^+$ and $\boldsymbol{R}^-$ are found. Note that φ is the phase in the complex plane.

$$\begin{cases} \boldsymbol{R}^+ = \frac{1}{2}[(a+d) + i(c-b)]e^{i\omega t} = |\boldsymbol{R}^+|e^{i\varphi_+}e^{i\omega t} \\ \boldsymbol{R}^- = \frac{1}{2}[(a-d) + i(c+b)]e^{-i\omega t} = |\boldsymbol{R}^-|e^{i\varphi_-}e^{-i\omega t} \end{cases} \quad [16]$$

Following the same method for the surface level, the pressure gradient vector $\boldsymbol{G}$ is rewritten as follows: $\boldsymbol{G} = \boldsymbol{G}^+ + \boldsymbol{G}^- = \frac{\partial \zeta}{\partial x} + i\frac{\partial \zeta}{\partial y}$. Then, by filling in the complex notations for u, v, $\frac{\partial \zeta}{\partial x}$ and $\frac{\partial \zeta}{\partial y}$ into the simplified equations of motion, and add (or subtract) both equations, the following equations are obtained:

$$\begin{cases} i(f+\omega)\boldsymbol{R}^+ = \boldsymbol{G}^+ + \frac{\partial}{\partial z}\left(E\frac{\partial \boldsymbol{R}^+}{\partial z}\right) \\ i(f-\omega)\boldsymbol{R}^- = \boldsymbol{G}^- + \frac{\partial}{\partial z}\left(E\frac{\partial \boldsymbol{R}^-}{\partial z}\right) \end{cases} \quad [17]$$

From these equations a solution for $\boldsymbol{R}^+$ and $\boldsymbol{R}^-$ can be found. The solution is assumed to be of the form $\boldsymbol{R}^\pm = [c_1 e^{-\alpha z} + c_2 e^{\alpha z} + c_3]e^{\pm i\omega t}$, and the expression is divided by the depth-averaged current $\langle u \rangle = \int_0^D u(z)dz$ (neglecting the varying surface ζ). The solution becomes:

$$\frac{\boldsymbol{R}^\pm}{\langle \boldsymbol{R}^\pm \rangle} = \frac{\cosh\left(\boldsymbol{\alpha}^\pm(z-D)\right) - \cos(\boldsymbol{\alpha}^\pm D) - \frac{\boldsymbol{\alpha}^\pm}{s}\sinh(\boldsymbol{\alpha}^\pm D)}{-\cos(\boldsymbol{\alpha}^\pm D) + (\frac{1}{\boldsymbol{\alpha}^\pm D} - \frac{\boldsymbol{\alpha}^\pm}{s})\sinh(\boldsymbol{\alpha}^\pm D)} \quad [18]$$

Where $\boldsymbol{\alpha}^\pm$ is the inverse of the boundary layer height $\boldsymbol{\delta}^\pm$:

$$\boldsymbol{\alpha}^\pm = (1+i)\sqrt{\frac{f \pm \omega}{2E}} = \frac{1}{\boldsymbol{\delta}^\pm} \quad [19]$$

B.2 ELLIPSE PROPERTIES

From the solutions $\boldsymbol{R}^{\pm}$ the main properties of the ellipse can be derived: the major and minor axis, the inclination (ψ) and the phase (φ).

$$\begin{cases} A_{major} = |\boldsymbol{R}^{+}| + |\boldsymbol{R}^{-}| = \frac{1}{2}|(a+d) + i(c-b)| + \frac{1}{2}|(a-d) + i(c+b)| \\ A_{minor} = |\boldsymbol{R}^{+}| - |\boldsymbol{R}^{-}| = \frac{1}{2}|(a+d) + i(c-b)| - \frac{1}{2}|(a-d) + i(c+b)| \\ \psi = \frac{1}{2}(\varphi_{+} + \varphi_{-}) = \frac{1}{2}\arg\left(\frac{1}{2}[(a+d) + i(c-b)]\right) + \frac{1}{2}\arg\left(\frac{1}{2}[(a-d) + i(c+b)]\right) \\ \varphi = \frac{1}{2}(\varphi_{+} - \varphi_{-}) = \frac{1}{2}\arg\left(\frac{1}{2}[(a+d) + i(c-b)]\right) - \frac{1}{2}\arg\left(\frac{1}{2}[(a-d) + i(c+b)]\right) \end{cases} \quad [20]$$

C. THE MATLAB FUNCTION PRANDLE_1982

The Matlab function Prandle_1982 was written by Gerben de Boer and gives the normalised tidal velocity profile at a specific location. The function has three different methods to obtain this result, each giving exactly the same result. The first two methods follow the derivation explained by de Boer (de Boer, Pietrzak and Winterwerp 2006), which was used in the second chapter, the third method uses the (outdated) implicit method as introduced by (Prandle 1982a). It doesn't matter which method is chosen.

C.1 OUTPUT

The desired result is the normalised tidal velocity profile in the form of a column vector. Each row in the column vector represents a height along the vertical between bottom and surface. Each element contains information about the magnitude and the direction of the tidal current at that specific location at the position along the vertical corresponding to that row. This information is presented as a complex number, where the real part represents the alongshore component, and the imaginary part the cross-shore component. The normalised velocity is the sum of both components: $U0 = u + iv$. If the real velocity is desired, the normalised velocity profile $U0$ needs to be multiplied with the depth-averaged velocity $U_{depthavg}$.

The way the function is used for this project, the normalised tidal velocity is not the direct outcome of Prandle_1982. The output of the function is one of the two phasors making up the velocity vector. As explained in appendix B, the tidal velocity U can be split up into two counter rotating phasors: $\boldsymbol{U} = \boldsymbol{R}^+ + \boldsymbol{R}^-$. The depth-averaged cross-shore velocity is assumed to be zero, because of the proximity of the coastal wall. Therefore, when $\boldsymbol{R}^+$ and $\boldsymbol{R}^-$ are in anti-phase, which happens for $t = \frac{T}{4}$ and $t = \frac{3T}{4}$, the depth-averaged cross-shore velocity needs to be zero: $U_{cross-shore} = |\boldsymbol{R}^+| - |\boldsymbol{R}^-| = 0$. When $\boldsymbol{R}^+$ and $\boldsymbol{R}^-$ are in phase, at $t = 0$ and $t = \frac{T}{2}$, there is no cross-shore component, therefore the depth-averaged alongshore velocity must equal the depth-averaged velocity: $U_{alongshore} = U_{depthavg} = |\boldsymbol{R}^+| + |\boldsymbol{R}^-|$. Combining both equations means that $|\boldsymbol{R}^+| = |\boldsymbol{R}^-| = \frac{|U_{depthavg}|}{2}$. So, in order to obtain $\boldsymbol{R}^+$ or $\boldsymbol{R}^-$, the result given by Prandle_1982 should be halved. Depending on the input, Prandle_1982 either gives $\boldsymbol{R}^+$ or $\boldsymbol{R}^-$. The normalised tidal velocity profile is then obtained by adding both phasors, and eventually multiplied with $U_{depthavg}$ for the real tidal velocity profile.

C.2 INPUT

The function needs a set of parameter values characterising the specific location for which the normalised tidal velocity profile is required. First parameter is the depth D, in m, the distance from the bed to the surface, ignoring small scale bed and surface variations. The second input parameter is the eddy viscosity coefficient E, in m^2/s. It is important to note that, for the analytic solution, the eddy viscosity is assumed constant over the entire depth. Next a column vector z is given, which defines the heights at which $U0$, the normalised tidal velocity, should be sampled. The first element of this vector is the lowest height, the last element is the height closest to the surface. The fourth input determines whether Prandle_1982 will give the positive or negative phasor. For the positive

phasor R^+, we give $f + \omega$, for the negative phasor R^-, we give $f - \omega$. Here f is the Coriolis parameter, where the f-plane assumption is made (see appendix A), which means that the Coriolis force is constant with latitude in our domain. In this case, f is defined as $f = 2 * \Omega * \sin(\varphi)$, where Ω is a constant representing the angular velocity of rotation of the Earth, with $\Omega = \frac{2\pi}{1\ day} = 7.2921 * 10^{-5} \frac{rad}{s}$ and φ is the average latitude of the considered domain (52° for the Rhine ROFI).

The next input parameter is the depth-averaged velocity $U_{depthavg}$, in m/s, and the last parameter is the bed friction parameter k, a dimensionless friction constant.

C.3 MATLAB SCRIPT

```
function U0 = prandle_1982(D,E,z,w,Udepthavg,k)
%PRANDLE_1982 tidal velocity profile of Prandle 1982
%
% U0 = prandle_1982(D,E,z,w,Udepthavg,k) returns the
% normalized tidal velocity profile U0 = U(z)/avg(U) where
% D [m]             the depth
% E [m2/s]          the constant eddy viscosity,
% z [m]             the height where U0 should be sampled
% k [-]             a friction constant
% w [rad/s] (omega) the radial frequency and
% Udepthavg [m/s]   the depth averaged current.
%
% Do not forget to multiply the result U0 with Udepthavg to obtain real velocities.
%
%   --------------------------------------------------------------------
% $ Id: prandle_1982.m 8518 2013-04-26 07:55:16Z boer_g $

% $ Author: boer_g $

% $ HeadURL:
https://svn.oss.deltares.nl/repos/openearthtools/trunk/matlab/general/phys_fun/prandle_1982.m
$

% explicit one-line notation version 2 of de Boer et al, 2006: dx.doi.org/10.1007/s10236-005-
0042-1

   s  = 8.*k.*abs(Udepthavg)./(3.*pi.*E);

   a  = (1+1i).*sqrt(w./(2.*E));

   U0 = (cosh((z-D).*a) - cosh(D.*a) + (          - a./s).*sinh(D.*a))./...
        (               - cosh(D.*a) + (1./(a.*D) - a./s).*sinh(D.*a));
```

D. INFLUENCE OF THE EDDY VISCOSITY COEFFICIENT ON THE VELOCITY PROFILE

D.1 INFLUENCE OF THE EDDY VISCOSITY COEFFICIENT

The eddy viscosity coefficient is used for turbulence modelling. The eddy viscosity coefficient E represents on a larger scale the transport and dissipation of energy due to small-scale turbulence. A large value for E means much turbulence, smaller values represent less turbulence. In this project, the eddy viscosity coefficient is assumed to be constant over the entire depth.

Figure 14 illustrates the influence of the value chosen for this constant E on the velocity profile. It is obvious that it has a big influence on the ellipticity. For a high E (lower row: $E = 0.04\ {}^{m^2}/_{s}$), the tidal motion becomes almost rectilinear. For a smaller value for E (upper row: $E = 0.004\ {}^{m^2}/_{s}$), the tidal motion shows a clear elliptic behaviour.

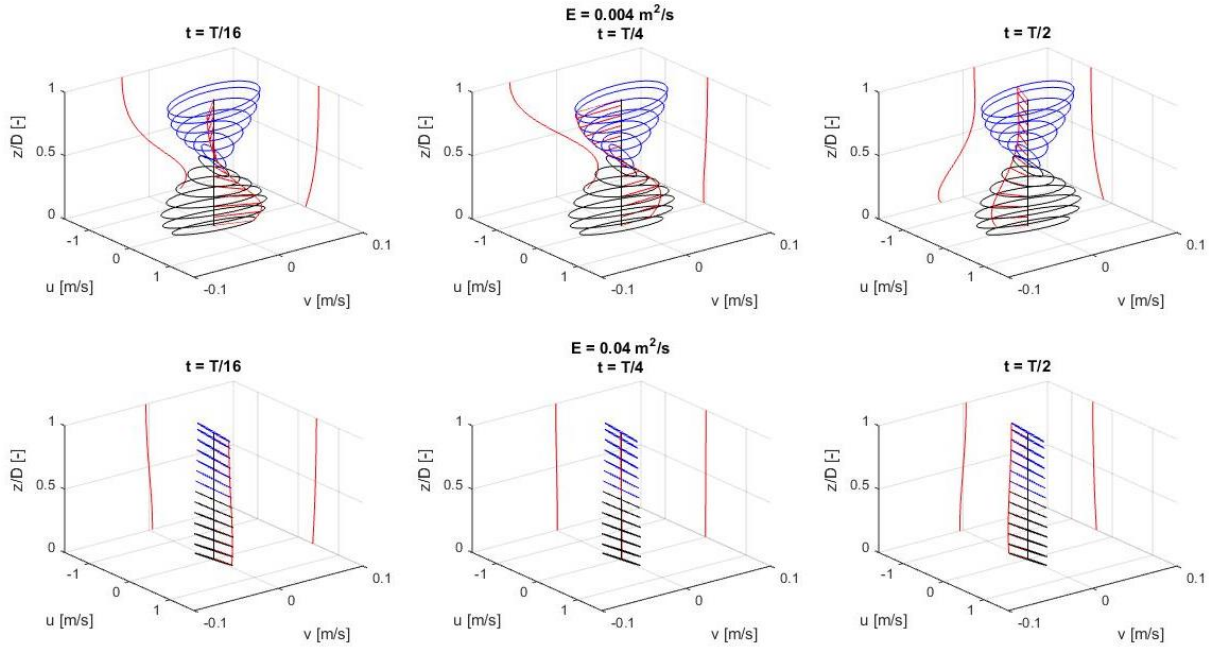

FIGURE 14: VERTICAL VELOCITY PROFILE FOR DIFFERENT VALUES FOR E. UPPER ROW: E = 0.004 M²/S, LOWER ROW: E = 0.04 M²/S.

D.2 Influence of the eddy viscosity coefficient integrated in the tidal cycle

The above plots were created while changing the value for E, but keeping all other input parameters the same. The values for E where chosen in order to show the difference in behaviour. This is good to understand the influence of E, but may be far from a real situation.

For a more realistic image, it is a good idea to look at the difference between spring and neap tide in the Rhine ROFI. The difference between spring and neap tide is the depth-averaged velocity: at neap tide, $U_{depthavg} = 0.43\,{}^{m}/_{S}$, while at spring tide, $U_{depthavg} = 0.66\,{}^{m}/_{S}$. Using Bowden's relationship between E and D: $E = \alpha * U_{depthavg} * D$, for $\alpha = 0.0012$, the eddy viscosity coefficient at neap tide is $E = 0.01\,{}^{m^2}/_{S}$ and at spring tide $E = 0.015\,{}^{m^2}/_{S}$. This results in the next series of plots in Figure 15.

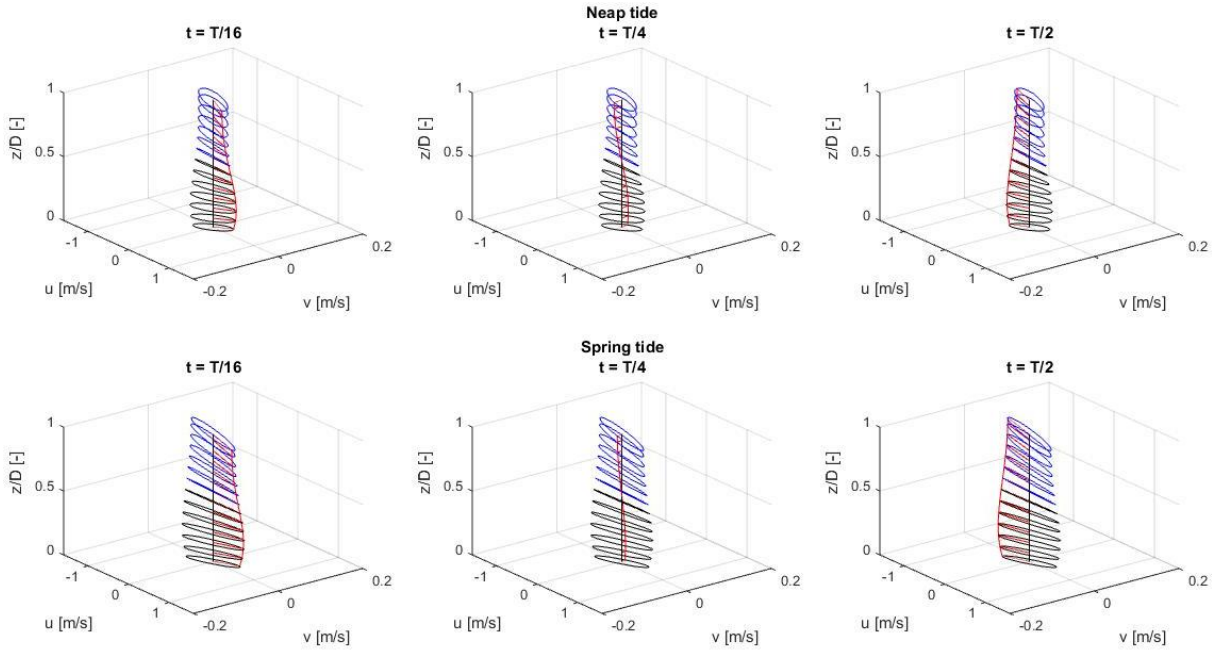

Figure 15: Vertical velocity profiles at the Rhine ROFI, upper row represents neap tide, lower row spring tide.

It is clear from these plots that for neap tide a nice elliptic behaviour occurs, but for spring tide the tidal motion becomes almost rectilinear. A small change in eddy viscosity therefore can lead to a big difference in behaviour, from stratification to mixing over the entire vertical, from elliptic behaviour to a rectilinear motion.

D.3 VELOCITY PROFILES FOR RANGE OF EDDY VISCOSITY COEFFICIENTS

The next plots show the amplitude structure and phase structure over depth for a range of values of the eddy viscosity coefficient E. On the horizontal axis of Figure 16 one can see the range of eddy viscosities, while the vertical axis represents the normalised height in the water column.

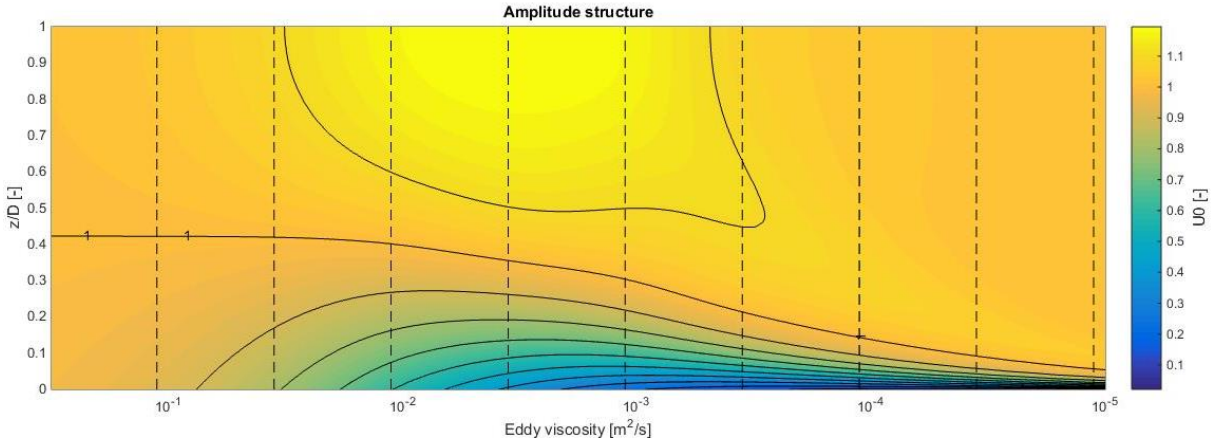

FIGURE 16: AMPLITUDE STRUCTURE FOR A RANGE OF EDDY VISCOSITY COEFFICIENTS, E RANGING FROM 1 M²/S TO 10E-05 M²/S.

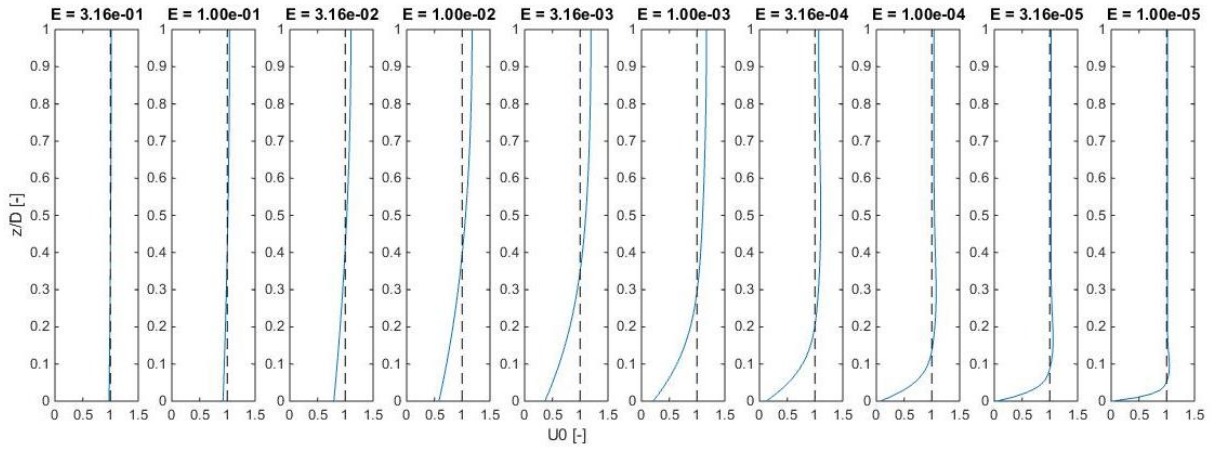

FIGURE 17: AMPLITUDE PROFILES FOR A SET OF EDDY VISCOSITY COEFFICIENTS. EACH VALUE FOR E IS REPRESENTED BY DOTTED VERTICAL LINE IN FIGURE ABOVE.

For large and intermediate values of E the amplitude changes with depth. For very small values of E, there's only a change in amplitude in a small layer near the bed. All water above this boundary layer moves at a more or less constant speed close to the depth-averaged velocity. The eddy viscosity coefficient for the Rhine ROFI is around $E \approx 0.01\, {}^{m^2}/_{s}$, which is the fourth plot from the left in Figure 17. The same plots can be given for the phase structure, where the phase is expressed with respect to the surface layer, see Figure 18 and Figure 19.

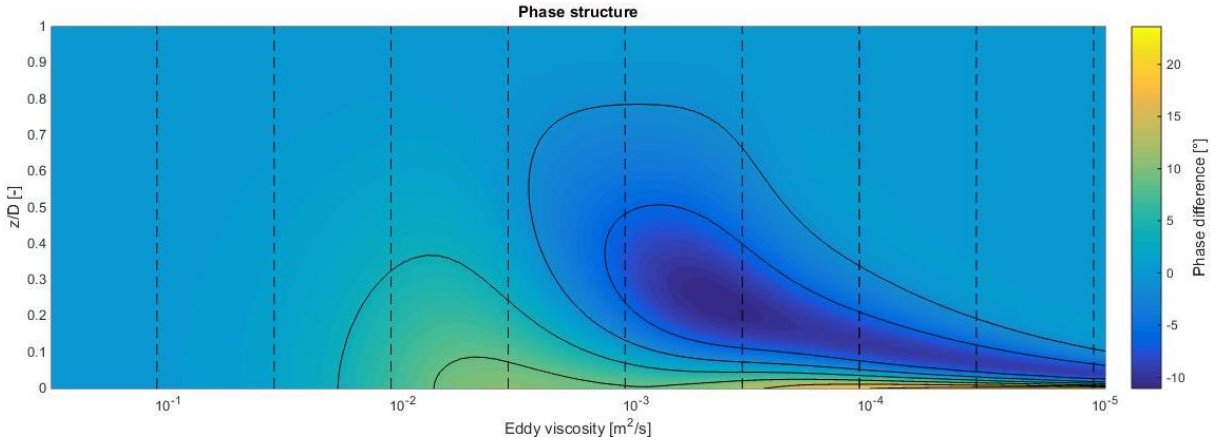

FIGURE 18: PHASE STRUCTURE FOR A RANGE OF EDDY VISCOSITY COEFFICIENTS, E RANGING FROM 1 M²/S TO 10E-05 M²/S.

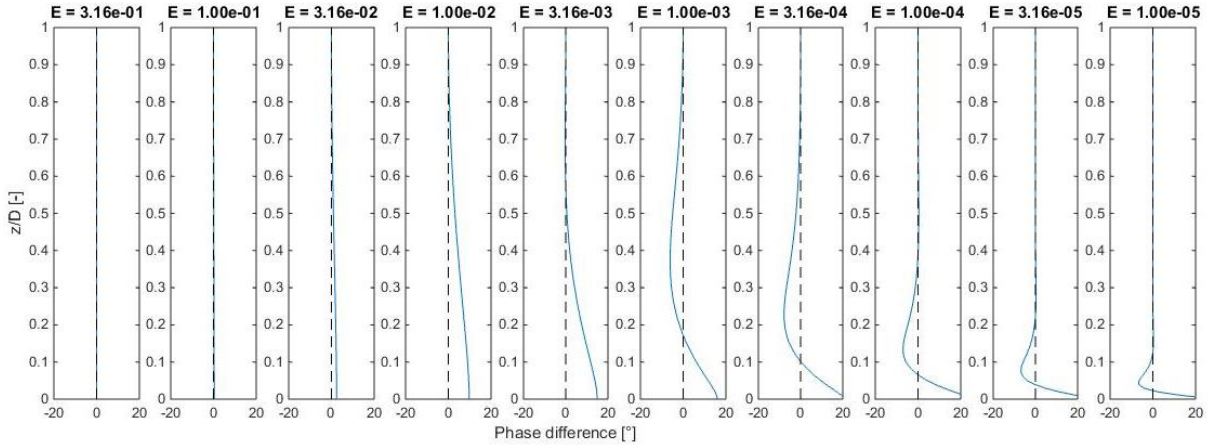

FIGURE 19: PROFILES FOR A SET OF EDDY VISCOSITY COEFFICIENTS. EACH VALUE FOR E IS REPRESENTED BY DOTTED VERTICAL LINE IN FIGURE ABOVE.

From these plots it can be said that there are different zones of behaviour. For very large eddy viscosity coefficients ($E \geq 0.1\, {}^{m^2}/_{s}$), there is no phase difference, the entire water column moves at the same phase. For slightly smaller values for E ($0.1\, {}^{m^2}/_{s} > E > 0.003\, {}^{m^2}/_{s}$), the phase starts taking a lead on the phase at the surface, the lead growing along the vertical, being maximum at the bed. This is the situation at the Rhine ROFI (fourth plot from the left in Figure 19). For even smaller values ($E \leq 0.003\, {}^{m^2}/_{s}$), there are three layers of different behaviour: the upper layer where there is no phase difference, a middle layer where the phase lags behind, and the lower layer near the bed where the phase is ahead of the phase at the surface. For decreasing values of E, the two lower layers become smaller and the upper layer with no phase difference determines the behaviour of almost the entire water column, with exception of a small boundary layer near the bed where the phase first lags behind and then takes a lead on the phase at the surface. The Fraser is expected to be in this last case.